

Characteristics of autoignition sites in turbulent non-premixed flows

C.N. Markides, E. Mastorakos

*Hopkinson Laboratory, Department of Engineering,
University of Cambridge, U.K.*

Full-length article submitted to:
Combustion and Flame

Corresponding Author:

E. Mastorakos

Hopkinson Laboratory,

Department of Engineering,

University of Cambridge,

Cambridge, CB2 1PZ, U.K.

Telephone: + 44 (0) 1223 332690

Fax: + 44 (0) 1223 332662

E-mail: em257@eng.cam.ac.uk

Short Running Title: "Characteristics of autoignition sites"

Sent: January 23, 2006

Abstract

Autoignition of acetylene and pre-vapourised heptane plumes in hot turbulent air has been visualised by monitoring OH^* chemiluminescence with a fast intensified camera and a photomultiplier. Autoignition occurred randomly in isolated spots whose location moved downstream with increasing air velocity or lower air temperature. The timescales associated with the repeated occurrence of these spots, the rise of the OH^* signal due to localised autoignition, and its subsequent decay due to the propagating flamelets around these localised ignitions have been quantified. The mean duration between autoignition events decreased with increasing air temperature and velocity. The OH^* timeseries and the fast-camera visualization reveal the emergence of secondary spots immediately adjacent to a primary event, which result in a long integral timescale of the OH^* signal when autoignition happens close to the injector. Examination of the films identified the location of individual spots and it was found that the r.m.s. of the axial position of the spots was in quantitative agreement with our expectations from the combination of turbulent dispersion of fuel and the inlet air temperature fluctuations. The data are consistent with insights from DNS and can provide a useful validation test for advanced unsteady turbulent combustion models.

1 Introduction

The autoignition of turbulent inhomogeneous mixtures when the air is hotter than the fuel controls the operation of diesel engines and is important in some modern lean-burn gas turbines, where autoignition in the premixing ducts must be avoided. To illustrate how turbulence can affect the emergence of autoignition in such flows, and the difficulties involved in theoretically predicting these effects, consider first a laminar strained layer between hot air and colder fuel. Ignition will occur at a preferred mixture fraction, denoted as the “most reactive mixture fraction”, ξ_{MR} [1, 2]. This mixture fraction is determined by the chemistry, the dilution, the temperatures of the two streams [1–4] and the scalar dissipation rate N ($N = D(\partial\xi/\partial x_i)^2$), with high values of N shifting ξ_{MR} to richer values [4–6]. As a paradigm of what may happen in turbulent flows, calculations showed that autoignition of a non-premixed flame in the presence of a vortex can occur in the strained layer or in the centre of the vortex depending on the relative magnitude of the chemistry and the vortex timescale [7]. In addition to vorticity, turbulence creates regions of high and regions of low scalar dissipation rate and the DNS data [1, 2] showed that the latter regions autoignite first. It was also evident that autoignition is likely to occur in the centre of vortical structures in a turbulent flow because the conditional scalar dissipation can become very low there due to the intense mixing achieved [2]. These findings have been substantially extended by many simulations with simple and complex chemistry in two- [8–12] and three-dimensional turbulence [13] and in vortical laminar flows [14]. It seems that all simulations agree that autoignition occurs at ξ_{MR} and at the lowest value of the scalar dissipation rate conditional on ξ_{MR} , $N|\xi_{MR}$, which could be located either inside a vortex or in a layer with low strain rate.

There is less agreement concerning how the turbulent velocity and integral lengthscale can affect the *time* of the first appearance of an autoignition site. Mastorakos et al. [1] conjectured that both these quantities affect the ignition delay time through their action on the mean value and the fluctuations of $N|\xi_{MR}$. Steep initial gradients of mixture fraction cause high initial values of $N|\xi_{MR}$. These values may remain high throughout the induction period, with a resulting prolongation of the autoignition delay time relative to the ignition time of the most reactive homogeneous mixture, or they may decay quickly if the turbulence is intense or the

scalar lengthscale small, hence reducing this prolongation effect.

There have been very limited *experimental* investigations on how turbulence can affect autoignition location and timing. In an experiment with spray injected in hot air, background turbulence accelerated autoignition [15], consistent with diesel engine data [16] that show a reduced ignition time with increasing engine speed. Modelling of spray autoignition with Conditional Moment Closure (CMC) [5] reproduced the conjecture of Refs. [1, 2] that although $N|\xi_{MR}$ may be higher initially in the turbulent flow, it decays faster and hence autoignition is facilitated. A turbulent counterflow between hot air and diluted fuel has been studied experimentally with hydrogen [17, 18] and heptane [19]. Both these experiments showed that the minimum air temperature necessary to observe autoignition increases as the turbulent velocity fluctuations increase, which suggests a retardation of the pre-ignition reactions.

The experiments in the opposed-jet flow did not directly measure autoignition times, because the experimental observable was the limiting condition at which ignition was precluded, rather than a quantification of where and when ignition may occur in a turbulent flow. In an effort to provide additional experimental data that can further our understanding and can assist the validation of theoretical models, autoignition of hydrogen in a turbulent co-flow of hot air in a duct was examined [20]. The fuel and air velocities were independently controlled, as was the air temperature. The novelty of that experiment lied in the use of a turbulent flow reactor with autoignition happening in the non-premixed, rather than in the well-mixed region. (The latter arrangement would provide data only for chemical kinetics validation.) The main findings of Ref. [20] were that: (i) there is a range of air and fuel velocities and temperatures where a statistically-steady situation exists with individual autoignition spots appearing in random locations, with flamelets growing from them that then decay; and (ii) the length along the duct where these spots occur increases fast with the flow velocity, suggesting that the mean residence time until autoignition increases with velocity.

The latter result is consistent with the counterflow experiments [17] and is further explored in this paper. It can be explained by the increasing scalar dissipation when the velocity increases and has been successfully reproduced with CMC modelling of this flow [6]. The former result comprises a new observation in autoignition in inhomogeneous flows and this regime of operation was called “random spots” [20]. The flamelets that emanated from the autoignition sites did not

result in full flame establishment, unlike in virtually all the DNS studies where a flame along the whole mixing layer always followed localised autoignition and unlike the fuel jets in hot vitiated air that stabilise a lifted flame [21]. The existence of randomness in the location of autoignition spots in turbulent flows may be expected, since the spatial locations where $N|\xi_{MR}$ is small are expected to be spread out and since we expect a statistical distribution of local curvature of the fuel-air interface that promotes the focusing of radicals [8, 10, 19]. Autoignition spots have also been visualized in diesel engines [16] as a function of air speed and temperature and a large scatter in ignition location along the spray was found.

In the present paper, some further characteristics of the random spots regime are presented to assist our understanding and to quantify better the randomness of ignition location. It is expected that the availability of such data will help the validation of advanced turbulent combustion models such as those based in transported PDF and LES methods. In addition, hydrocarbon fuels are tested to avoid differential diffusion effects that have been shown to be important for hydrogen autoignition [8, 22], but not so much for heptane [23]. The particular objectives are: (i) to investigate the autoignition behaviour of acetylene and pre-vaporized n-heptane in inhomogeneous turbulent flows; (ii) to report more details on the statistics of autoignition site locations; (iii) to characterize the timescales involved with the evolution of an autoignition spot; and (iv) to provide data that can assist model validation. The rest of the paper is organised as follows. In the next Section, the experimental arrangement is described and the measurement methods explained. Results concerning the ignition location and timescales are then presented and discussed. The paper closes with a summary of the most important conclusions.

2 Experimental Methods

Details of the apparatus, velocity, temperature, and mixture fraction measurements have been reported in Refs. [20, 24–26] and only the main features are repeated here. Figure 1 shows the experimental arrangement schematically. Filtered air from a compressor was heated electrically with feedback control so that the temperature at the exit of the heaters was kept within 1°C from the set value. A perforated plate with 44% solidity and circular holes of diameter $M=3$ mm was placed before the test section to enhance the turbulence and to provide a uniform velocity profile and a better controlled integral lengthscale. The test section comprised a 0.5 mm long quartz pipe of $D=25$ mm inner diameter. The pipe was vacuum sealed in a second concentric quartz pipe to minimize heat losses and was open to the atmosphere.

The fuels used were acetylene and pre-vapourised n-heptane. A mass flow controller was used for acetylene, while vapourised n-heptane was provided by a positive displacement peristaltic pump and a small electric heater. The fuel was mixed with nitrogen and was injected into the quartz tube axially and continuously through a 2.27 ± 0.03 mm inner (d) and 2.96 ± 0.02 mm outer (d_o) diameter, stainless steel tube, whose exit was 62 mm downstream of the perforated plate. For a few experiments presented in Section 3.5, a smaller injector of 1.03 mm inner diameter has also been used. The dilution is described by the mass fraction of fuel Y_{fuel} . For most of its length, the injector was encased in a 2.0 mm thick ceramic sheath to keep the fuel stream as cool as possible and hence minimize thermal decomposition. The fuel stream injection temperature (T_{fuel}) was measured with a 0.25 mm diameter Chromel/Alumel thermocouple that was placed through the injector all the way to the injection location. T_{fuel} was in the range 600 to 1100 K.

At the inlet of the quartz tube (26 mm upstream of the injector nozzle), a 0.2 mm diameter Pt/Pt&13%Rh thermocouple was used to measure the mean air temperature (T_{air}). At the exit of the tube, a second thermocouple was used to monitor heat losses and detect combustion. The raw T_{air} reading was corrected for both radiative and conductive heat losses from the thermocouple wires. Typically, after correction for these losses, the reported T_{air} has an indeterminate uncertainty of $\pm 0.3\%$ and a determinate uncertainty of $\pm 0.6\%$. Air with T_{air} up to 1200 K has been used. Despite the elimination of conduction losses in the vacuum-sealed tube, the centreline temperature drops linearly by 10 K in the first 100 mm.

The bulk air velocity (U_{air}) varied between 10 and 35 m/s, while the fuel velocity (U_{fuel}) was set approximately equal to U_{air} so that $v_{fuel} = U_{fuel}/U_{air} = 1 \pm 0.2$. A Dantec constant temperature hot wire was used to measure the axial velocity at cold conditions, but at the same bulk Reynolds number ($U_{air}D/\mu$) as the hot flows, with and without flow from the injector. In order to estimate the turbulent temperature fluctuations that may be present in the air stream, a 76 μ m diameter, K-Type thermocouple wire was employed with compensation for the time constant of the wire (≈ 40 ms) performed in the frequency domain. The rms of the temperature fluctuations, $(\overline{T'^2})^{1/2}$, was hence found to be about 0.25% of T_{air} for the conditions of this paper [24]. This corresponds to about 2.5 K in actual autoignition conditions. We will refer to this estimate later when we discuss the reasons for the observed randomness of autoignition locations.

After T_{air} reached the desired temperature, the fuel and nitrogen flow rates were adjusted and autoignition was detected in the tube. A Hamamatsu photomultiplier tube (PMT) with a 307 ± 10 nm filter was used to collect OH* chemiluminescence from the whole flow and the PMT voltage was amplified, sampled at 100 kHz and stored on a computer. Sampling times varied from 10 s to 80 s in order to capture enough events and ensure adequate convergence of statistics. A high-speed, 10-bit Phantom v.4.2 CMOS camera and a C9546-04MP46 Hamamatsu intensifier was used to provide planar chemiluminescence images. Typically, 512x152 pixel images were collected at frame rates of up to 12 kHz. A UV-lens (focal length 105 mm) and two optical filters (Melles Griot UG11 and a filter at 307 ± 10 nm) were used. The raw images from the CMOS camera were first processed to remove noise. Some of the fast movies were examined manually from which the following information was extracted: (i) the location of the first appearance of light emission from a completely dark background; and (ii) the speed of propagation of the flamelet emerging from the autoignition spot. Item (i) is discussed in detail later in this paper, while Item (ii) has been presented in Ref. [25].

Pressure fluctuations in the tube were measured with a Brüel&Kjær microphone assembly, consisting of a 1/4" Type 4135 free-field acoustic transducer, a 1/4" 2633 preamplifier and a 2807 power supply. The microphone was placed at the inlet of the quartz tube. The signal was taken from the microphone to the power supply, after which it was amplified, low-pass filtered and recorded by the PC. The microphone measurements were made simultaneously with

the PMT. The autocorrelation coefficient of the PMT instantaneous voltage $V(t)$ was used to calculate the integral timescale and the Taylor microscale using the method of Ref. [27]. It will be apparent from the results that both $V(t)$ and the microphone pressure signal, $P(t)$, were highly intermittent, which in most cases allowed the identification of individual autoignition events. The statistics of the temporal spacing between such events were determined.

3 Results and Discussion

3.1 Initial conditions and mixing

The velocity measurements showed that $\bar{U}/U_{air} \approx 1.10 - 1.15$ away from the tube and injector walls. Similarly, u'/\bar{U} (u' is the rms of the axial velocity fluctuations) was found to be around 0.12 – 0.15 at the inlet, decaying to 0.10 at a distance of $x = 42$ mm downstream and was relatively uniform across the pipe. The integral timescale in the air flow was measured and, using Taylor’s hypothesis, provided an estimate of L_{turb} between 3 and 4 mm across the tube at the inlet, i.e. of the order of the grid hole size, increasing by approximately 1 mm in the first 42 mm downstream. The turbulent Reynolds number ($Re_{turb} = u'L_{turb}/\nu$) varied between 50 and 100.

Previous acetone PLIF measurements [26] showed that the mixture fraction, defined as unity in the fuel stream and zero in the air stream, decayed as expected from analytical results for the diffusion from a point source in uniform mean flow with homogeneous turbulence, for axial distances at least up to about 50 mm downstream of the injector, which was where the fuel plume reached the walls. Downstream of this, the confinement was evident. The mean mixture fraction field did not depend on U_{air} , since $U_{fuel} \approx U_{air}$, the diffusivity scaled with U_{air} , and L_{turb} was independent of U_{air} . The mean and r.m.s. of the mixture fraction have been successfully predicted with standard CFD methods [6].

3.2 Qualitative observations

The results reported in this section are similar for all fuels studied and repeat some findings from Refs. [20, 24] to clarify the phenomena. Depending mostly on the air velocity and temperature and the fuel velocity, different behaviours were observed. At very low temperatures, no autoignition was observed. At very high temperatures, flashback and the establishment of an attached non-premixed flame was unavoidable. For a range of operating conditions, randomly-located spots were observed. This is the “Random Spots” autoignition regime. Operation in this mode resulted in continuous, recurring autoignition spots accompanied by a popping sound. Figure 2 shows direct photographs of these spots taken with a conventional digital camera. It is evident that flamelets appear randomly spread across and along the tube. There is no continuous flame

sheet and the base of the individual flamelets may be thought to resemble triple flames, which have been previously observed in simulations of various autoignition problems [1, 28].

From long-exposure images similar to that in Fig. 2c, the minimum axial location where autoignition occurs, X_{MIN} , has been reported as a function of air temperature and air and fuel velocities for hydrogen [20] and for hydrocarbon fuels later in this paper. As T_{air} increased or U_{air} decreased, the ignition location moved closer to the fuel nozzle and the radiated chemiluminescence was intensified and the associated noise increased in pitch and loudness. The global appearance shifted from blue to bright yellow for acetylene or more orange-yellow for heptane. Emission spectra revealed peaks associated mainly with OH^* , CH^* and C_2^* , while a broad content associated with formaldehyde was also detected for T_{air} slightly lower than that necessary to cause autoignition inside the tube [24].

High-speed images (Fig. 3) showed the following. For conditions where autoignition happened downstream in the tube, individual regions of high light intensity emerged from a completely dark background and a spherical flamelet seemed to emanate from the spots. For example, Frames 2 and 4 in Fig. 3 show the individual, small spots, while the larger region in Frame 3 is the flamelet around the spot of Frame 2. These flamelets were convected with the flow and their luminosity decreased with time from autoignition or as they approached the wall. There could be a period of inactivity (e.g. the completely dark Frame 1, Fig. 3), and then another spot emerged elsewhere, e.g. compare Frame 2 with 4 and Frames 14 to 15 in Fig. 3. For conditions for which autoignition happened closer to the nozzle, the spots were less separated in space and time, but kept their individual nature. Even at conditions where ignition was closest to the injector, the high-speed images show individual sites, although they were now occurring simultaneously at different locations and were in close proximity, as in Frame 16 of Fig. 3.

Such high-speed movies have been analyzed manually to measure the axial (X_{IGN}) and radial (Y_{IGN}) coordinate of individual autoignition spots, which are taken to be the locations of the first emergence of a small luminous spot from a dark image (e.g. the circled spots of Fig. 3, Frames 2, 4, 15). The statistics of these locations quantify the randomness in autoignition location. Note that since these are line-of-sight images, Y_{IGN} is the cross-stream projection of the radial location. These results are presented later in the paper. Although the particular images shown in Fig. 3 were taken with the small injector, all qualitative observations discussed

here were identical with the larger injector too.

3.3 Autoignition lengths

Figure 4 shows that autoignition of acetylene occurs between 30 and 120 mm from the nozzle, depending on the air velocity and temperature. As T_{air} increases, the minimum autoignition length, X_{MIN} , decreases, whereas as U_{air} increases, X_{MIN} increases. For lower temperatures than the ones used here, no autoignition was observed at all in the tube. Decreasing Y_{fuel} increases the ignition length, as expected.

A residence time until X_{MIN} can be calculated as X_{MIN}/U_{air} and both the hydrogen [20] and the present acetylene data show that this time increases with U_{air} . This is also evident from Fig. 4 where, for example for $T_{air}=869$ K, X_{MIN} increases from 30 mm to 90 mm for an increase in U_{air} from 16 m/s to 24 m/s. Part of this increase may be understood by the reduction in mean air temperature along the tube. For example, if there was no retardation of the ignition delay *time* with U_{air} , we would expect, for the same example, that at $U_{air}=24$ m/s, X_{MIN} would be $24/16 \times 30$ mm = 45 mm. At this axial location, the mean air temperature may have decreased relative to $x=30$ mm by about 1.5 K due to heat losses. From the sensitivity of length to the air temperature (1.5 mm per K; Fig. 4b), this temperature reduction would correspond to an increase in length of about 3 mm. This accounts only for a small part of the observed increase. Hence, the conclusion of Ref. [20] that fast flow seems to delay autoignition of hydrogen is extended here to acetylene. The same conclusions have been reached by calculating a mean residence time from the average location of the autoignition spots, $\langle X_{IGN} \rangle / U_{air}$.

Similar trends have been found for heptane, Fig. 5. For example, in the neighbourhood of $T_{air}=1115$ K, X_{MIN} approximately doubles for an increase in U_{air} from 13.8 to 17.6 m/s. Modelling of the heptane data [6] showed that in these experiments, the conditional scalar dissipation $\langle N | \xi_{MR} \rangle$ is higher than the critical value necessary to preclude autoignition only for about the first 20-30 % of the length along the tube until the ignition point. This region where the scalar dissipation is higher than the critical value is longer for the data at the higher U_{air} used, which explains why X_{MIN}/U_{air} increases with velocity.

3.4 Chemiluminescence and pressure

Figure 6 shows the OH* chemiluminescence registered with the PMT simultaneously with a high-speed movie. Immediately before the explosion event, the camera records a dark background and the PMT records zero signal. Following autoignition, flamelets propagate radially outwards in all directions and the size of the reacting region grows, but the chemiluminescence intensity decreases. The explosive emergence of chemiluminescence occurs in around 0.5 ms. The post-ignition decay takes about 3 ms to reach 10% and 6 ms to reach 3% of the peak value.

Figure 7 shows typical timeseries of OH* and sound recorded for a situation with long and short X_{IGN} . The experiment with short X_{IGN} produces spotting more often, hence called “fast spotting”. It is evident that the “slow spotting” flow produces well-defined autoignition events, which are detected by both a sharp rise in the global OH* emission and a pressure burst above a relatively quiet background. Quite often, each spot has secondary peaks coming very close after the primary rise. We believe that some of these secondary peaks in the OH* signal are due to localized autoignition triggered by the narrow proximity of an earlier autoignition event, i.e. autoignition assisted by the flamelet propagation following from autoignition elsewhere. This is better shown in the sequence of Fig. 3, where an independent small spot is evident in Frame 15, the flamelet growth around it in Frame 16, and a second explosive spot next to the flamelet in Frame 16. Autoignition events separated by a large distance are also evident, e.g. Frame 4 in Fig. 3, which may also produce OH* peaks quite closely spaced in time.

In the “fast spotting” regime, it is difficult to distinguish between individual events, although a close examination of the time-series shows the same features of an explosive rise of OH* and a slower decay, which is interrupted by another sharp rise. Note the much higher pressure fluctuations and the higher instantaneous OH* intensity of each spot in the “fast spotting” flow, which is perhaps due to the fact that, since “fast spotting” occurs at short X_{MIN} , the autoignition spots are convected in the field of view for a longer time and have ample time to burn all fuel available, at least in their immediate vicinity. This, together with the fact that more spots appear per unit time at short ignition length conditions, explains why the time-averaged OH* signal decreases quickly with increasing X_{MIN} (Fig. 8). The r.m.s. also decreases. A higher air velocity (and hence fuel flow rate since in these experiments $U_{fuel} \approx U_{air}$) gives

higher mean OH* due to the larger amount of fuel that is burning.

The time distance between spots can be characterized by measuring the time delay Δt_{ign} between peaks of the OH* signal (see Fig. 7). These have been located by a peak-detection algorithm. Figure 9 shows that all experiments (i.e. for all X_{MIN}) show a similar shape for the probability distribution function (PDF) of the time delay between peaks. The PDF peaks at about 0.5 ms and has a long tail at longer delays, which increases substantially as we move from a “fast spotting” to a “slow spotting” flow. It is also evident that the probability of peaks closer than about 0.2 ms is negligible and that this limit seems to be independent of the flow conditions. The mean frequency ($1/\langle\Delta t_{ign}\rangle$) decreases very fast as X_{MIN} increases (i.e. air temperature decreases), Fig. 9b, and ranges from about 2 Hz to about 2 kHz for the conditions tested. Increasing the air velocity makes the mean time distance between the spots to decrease.

The autocorrelation of the OH* signal (Fig. 10a) decays to zero for long and intermediate X_{MIN} , while a periodicity becomes evident for some very “fast spotting” experiments. This may be due to a weak coupling between the pipe acoustics and the combustion, not evident at intermediate or long X_{MIN} . Visualization at these conditions (i.e. very high T_{air}) showed that it is difficult to distinguish individual spots and that the flame now resembles the lifted flames in vitiated air of Ref. [21], although a continuous flame sheet is still not clearly evident.

The integral timescale and the Taylor microscale have been calculated from the autocorrelation coefficient. It is evident that both decrease as ignition moves away from the nozzle, with the integral timescale showing a more substantial change than the Taylor microscale (Fig. 10b). For short X_{MIN} , the OH* timeseries remains correlated over a longer period of time, which is about 3 ms. This decreases to about 1 ms at long ignition lengths. The Taylor microscale is between 0.3 and 0.5 ms for all experiments, values very close to the duration of the initial OH* rise when autoignition appears (i.e. the peak OH* in Fig. 6).

For the experiments with $U_{air}=11.1$ m/s in Figs. 8 to 10, the turbulent integral timescale is about 4 ms and changes little with downstream distance. In contrast, the OH* integral timescale and the frequency at which the autoignition events appear depend strongly on ignition location. A possible explanation for these observations is as follows. Firstly, at short X_{MIN} we observe more secondary ignitions following a primary event, which suggests a longer time of coherence of the OH* signal than at long X_{MIN} . Secondly, recall the finding from DNS that autoignition

is preferred at low values of the conditional scalar dissipation $N|\xi_{MR}$. Long X_{MIN} implies that ignition occurs at locations where the mean and variance of the mixture fraction have decreased and hence $N|\xi_{MR}$ is low. The spot size is hence large, since the mixture fraction gradients are small. At short X_{MIN} , the scalar dissipation is higher and hence the spot is smaller; this implies that a larger number of spots occurs per unit volume, and the combustion across the flow can show a coherence over a longer period of time. This is consistent with the high-speed images that show many simultaneous, but smaller, initial kernels at short X_{MIN} .

As U_{air} increases, the scalar dissipation increases at the same location, which causes faster flamelet propagation following autoignition. The faster flamelet speed at high N is readily predicted by mixture fraction based modelling and has also been measured directly from the present images [25]. This argument explains why the integral timescale of the OH* signal decreases slightly as the air velocity increases for the same X_{MIN} (Fig. 10b).

The fact that autoignition events can be triggered by an earlier nearby autoignition is relevant to HCCI engines, as this phenomenon has been considered responsible for the quick growth of the combustion zone across the cylinder visualised in such engines [29]. In the present experiments, the minimum time delay between such primary and secondary events is about 0.2 ms. With a speed of sound of about 650 m/s for the conditions tested, this corresponds to a distance of 13 cm. This is much longer than the physical distance between the spots, which is not longer than 25 mm. Hence, the induced ignition from the primary to a secondary spot is probably not due to a localised pressure wave, e.g. as in engine knock or a developing detonation, but due to diffusion or convection of heat associated with a propagating flamelet.

3.5 The randomness of autoignition sites

Figure 11 shows scatter plots of the axial and projected radial location of the first emergence of heptane autoignition. These measurements are not contaminated by the possibility of flamelet propagation from the kernel or from internal reflections because they have been manually assembled from play-back of the high-speed films such as those in Fig. 3 and it has been ensured that only the first appearance of light emerging from a completely dark background region is included, i.e. we sample only primary autoignition sites. Only spots smaller than about 2 mm have been included in Fig. 11 and isolated so that no light was evident at a distance closer than

10 mm from the spot. So, for example, only the single circled spots in Fig. 3 are considered. Figure 11 shows that significant scatter in the ignition location exists. The axial r.m.s. of ignition position, $\sigma_{x,ign}$, is between 8 and 11 mm for the heptane experiments with $d=2.27$ mm, with no clear trend with velocity or temperature (Table 1). The cross-stream r.m.s. $\sigma_{y,ign}$ is about 5 mm and occasionally spots are found close to the wall, since at these long lengths the fuel plume has grown to fill the whole pipe. Possible explanations for these observations are discussed below.

Assume that all fluid particles that eventually ignite to comprise Fig. 11 have “lived” in the flow for the same time. Their spatial distribution could then be readily calculated from the turbulent dispersion of matter from the fuel source (e.g. the “Taylor dispersion” problem at long times). The PLIF mixture fraction data [26] showed that a simple diffusion process is adequate to describe mixing in this flow and numerical simulations [6] showed that the decay of the mixture fraction in the pipe is reproduced with a turbulent diffusivity of $D_t = 2.16 \times 10^{-3}$ m²/s for the high velocity conditions of Fig. 11 and 1.65×10^{-3} m²/s for the lower velocity. The expected r.m.s. of the axial and radial locations is hence $\sigma_X = (2D_t t)^{1/2}$, with t the residence time taken as $\langle X_{IGN} \rangle / U_{air}$. So, for the conditions of Fig. 11, this calculation gives an r.m.s. of the fluid particle location between 3.7 and 4.8 mm. These estimates are consistently smaller than the measured axial spread and similar in magnitude to the cross-stream one (Table 1). Hence, the observed randomness in the axial direction is probably not only due to turbulent dispersion.

Consider now the initial air temperature fluctuations. They have an r.m.s. of about 2.5 K and can result in fluctuations of ignition length. As discussed in Section 3.3, Fig. 5 shows a sensitivity of ignition length to air temperature of about 3 mm per K for heptane and so the inlet temperature fluctuations would result in an r.m.s. length fluctuation of about $\sigma_T=7.5$ mm, which accounts for a large part of the observed axial scatter in Fig. 11.

The above arguments suggest that the observed randomness in the radial position are only due to turbulent dispersion, while the scatter in the axial position is about twice that and can be understood by considering turbulent dispersion and the inlet temperature fluctuations. Despite the fact that the temperature fluctuations are small in absolute terms, they are sufficient to provide an observable randomness in ignition location. Interestingly, the measured axial variance

agrees quite well with $\sigma_{x,ign}^2 = \sigma_T^2 + \sigma_X^2$, which suggests that the two reasons above are sufficient to explain the measured ignition spot scatter.

The data of Figs. 4 and 5 show an increasing residence time until the mean location of ignition, consistent with the observations in Ref. [20], and explained by the delaying effect of the high scalar dissipation rate at high U_{air} . This delaying effect is restricted to the early regions of the plume, before N decays well below the critical value, as revealed from CMC modelling [6]. It seems that the random fluctuations of strain rate during this period do not introduce a randomness in the ignition time, in full agreement with DNS results [1, 8] that showed very small ignition time fluctuations between different realizations. The explanation offered in Ref. [1] was that ignition occurs at the lowest values of N and these are bound to appear more or less at the same time, but in different locations in the flow. In the present case and in the absence of initial temperature fluctuations, this explanation is equivalent to expecting ignition to occur at the same residence time, but with a spatial spreading determined by turbulent diffusion.

The conclusions concerning the spatial distribution of autoignition spots have been confirmed with limited data from an experiment with acetylene injected from a smaller injector, Table 2. Again, the estimated σ_X is very close to the measured cross-stream r.m.s., with the axial r.m.s. being higher by about 80%. Ignition is now closer to the injector and both the streamwise and the cross-stream spreading are less than with the larger injector. Scatter plots (not shown here) do not include any spots close to the walls, since the shorter ignition lengths and the smaller injector imply a thinner plume. Introducing the sensitivity to the inlet temperature fluctuations, which for acetylene is about 1.5 mm per K (Fig. 4b), shows that the measured axial r.m.s. lies within 30% of $(\sigma_T^2 + \sigma_X^2)^{1/2}$. Although the agreement is not as good as with the larger injector, it seems that the axial spreading is not too different from what one would expect from the fuel dispersion and the air temperature fluctuations.

It is interesting to note that for the small injector data of Table 2, the average residence time $\langle X_{IGN} \rangle / U_{air}$ is independent of U_{air} , in contrast to the larger injector data (e.g. Figs. 4, 5). This behaviour has also been demonstrated in two-dimensional DNS [1] and reproduced by modelling [2]. It has been attributed to the fact that the very quick mixing allowed by the small lengthscale of the scalar injection relative to the turbulent eddies severely reduces the region where the scalar dissipation is higher than the critical value and also introduces low values of

$N|\xi_{MR}$ early. This reduces or even completely eliminates the retardation effect of turbulence on autoignition.

The present results suggest that the autoignition time involves a randomness mostly determined by the initial temperature fluctuations, while the randomness of autoignition position is additionally due to turbulent dispersion. In diesel engines, an additional cause for the observed scatter [16] is the turbulent droplet dispersion and the randomness induced by the turbulent motion on atomization. Large Eddy Simulations with advanced sub-grid closures and transported PDF models would greatly enhance our understanding of the present phenomena. Further experiments with simultaneous mixture fraction and reactive scalar measurements are necessary.

4 Conclusions

Plumes of pre-vapourised heptane and acetylene in heated turbulent air have been used as model situations of autoignition in non-premixed flows. Autoignition has been visualised with a fast intensified camera and a photomultiplier was used to monitor global OH* chemiluminescence. It was found that autoignition occurred in isolated spots whose location moved downstream with increasing air velocity and/or lower air temperature. The characteristic frequency of occurrence of these spots increased when ignition happened close to the nozzle (i.e. by increasing the air temperature) and increased with air velocity for the same ignition location. The emergence of chemiluminescence from a dark background occurred over a sharp rise lasting about 0.5 ms for all conditions tested, while the OH* signal also showed a slow decay associated with the propagation of flamelets after the localised autoignition. Secondary autoignition events often followed a primary event, but analysis of the time duration between these ignitions suggest that the secondary ignition is triggered by heat transfer and not by pressure waves. The r.m.s. of the axial ignition spot location was quantitatively consistent with our expectations from turbulent dispersion and the additional spreading expected from the initial air temperature fluctuations, hence suggesting that the randomness in the strain rate history of the fluid that eventually ignites is not responsible for the randomness in the observed ignition location, consistent with previous DNS results.

Acknowledgements

We acknowledge the assistance of Drs. I. Day and A. Riley of CUED with the measurement equipment. This work has been financially supported by the Engineering and Physical Sciences Research Council.

References

- [1] E. Mastorakos, T. Baritaud, and T. Poinsot. *Combust. Flame*, 109:198–223, 1997.
- [2] E. Mastorakos, A.P. Da Cruz, T. Baritaud, and T. Poinsot. *Combust. Sci. Technol.*, 125:243–282, 1997.
- [3] A. Linan and A. Crespo. *Combust. Sci. Technol.*, 14:95, 1976.
- [4] R. Knikker, A. Dauplain, B. Cuenot, and T. Poinsot. *Combust. Theory Modelling*, 175:1783–1706, 2003.
- [5] Y. M. Wright, G. de Paola, K. Boulouchos, and E. Mastorakos. *Combust. Flame*, 143:402–419, 2005.
- [6] C.N. Markides, G. De Paola, and E. Mastorakos. In *Mediterranean Combustion Symposium*, Lisbon, October 2005.
- [7] D. Thevenin and S. Candel. *Phys. Fluids*, 7:434–445, 1995.
- [8] R. Hilbert and D. Thevenin. *Combust. Flame*, 128:22–37, 2002.
- [9] H.G. Im, J.H. Chen, and C.K. Law. *Proc. Combust. Inst.*, 27:1047–1056, 1998.
- [10] T. Echekki and J.H. Chen. *Combust. Flame*, 134:169–191, 2003.
- [11] S. Sreedhara and K.N. Lakshmisha. *Proc. Combust. Inst.*, 28:25–34, 2000.
- [12] A. Vaggiano and V. Magi. *Combust. Flame*, 137:432–443, 2004.
- [13] S. Sreedhara and K.N. Lakshmisha. *Proc. Combust. Inst.*, 29:2051–2059, 2002.
- [14] X.L. Zheng, J. Yuan, and C.K. Law. *Proc. Combust. Inst.*, 30:415–421, 2005.
- [15] H.J. Koss, D. Bruggemann, A. Wiartalla, H. Backer, and A. Breuer. *IDEA Project Final Report*, 1992.
- [16] T.A. Baritaud, T.A. Heinze, and J.-F. Le Coz. *SAE Paper 940681*, 1994.
- [17] J.D. Blouch, C.J. Sung, C.G. Fotache, and C.K. Law. *Proc. Combust. Inst.*, 27:1221–1228, 1998.

- [18] J.D. Blouch and C.K. Law. *Combust. Flame*, 132:512–522, 2003.
- [19] C. Kortschik, S. Honnet, and N. Peters. *Combust. Flame*, 142:140–152, 2005.
- [20] C.N. Markides and E. Mastorakos. *Proc. Combust. Inst.*, 30:883–891, 2005.
- [21] R. Cabra, T. Myhrvold, J.-Y. Chen, R.W. Dibble, A.N. Karpetis, and R.S. Barlow. *Proc. Combust. Inst.*, 29:1881–1888, 2003.
- [22] J. D. Blouch, J.-Y. Chen, and C.K. Law. *Combust. Flame*, 135:209–225, 2003.
- [23] V. Gopalakrishnan and J. Abraham. *Combust. Flame*, 136:557–566, 2004.
- [24] C.N. Markides. *Autoignition in Turbulent Flows*. PhD thesis, University of Cambridge, 2005.
- [25] C.N. Markides and E. Mastorakos. In *ASME Turbo Expo*, Barcelona, Spain, June 2006.
- [26] C.N. Markides and E. Mastorakos. *Chem. Eng. Sci.*, To appear, 2006.
- [27] C. Renner, J. Peinke, and R. Friedrich. *J. Fluid Mech.*, 433:383–409, 2001.
- [28] P. Domingo and L. Vervisch. *Proc. Combust. Inst.*, 26:233–240, 1996.
- [29] P.G. Aleiferis, A.G. Charalambides, Y. Hardalupas, A.M.K.P. Taylor, and Y. Urata. *SAE Paper 05FFL-189*, 2005.

Table 1: Statistics of ignition locations for experiments with heptane with $Y_{fuel}=0.94$ and $U_{fuel} \approx U_{air}$ and comparison with the r.m.s. expected from Taylor dispersion. For all, the injector was $d=2.27$ mm.

	U_{air} (m/s)	T_{air} (K)	$\langle X_{IGN} \rangle$ (mm)	$\sigma_{x,ign}$ (mm)	$\sigma_{y,ign}$ (mm)	$(2D_{tt})^{1/2}$ (mm)
Run 1	13.79	1112	67.3	8.41	5.23	4.02
Run 2	13.73	1104	83.2	10.84	5.18	4.47
Run 3	18.02	1124	95.6	8.38	5.06	4.79
Run 4	17.89	1137	57.3	8.43	4.95	3.71

Table 2: Statistics of ignition locations for experiments with acetylene with $Y_{fuel}=0.77$ and $U_{fuel} \approx U_{air}$ and comparison with the r.m.s. expected from Taylor dispersion. For all, the injector was $d=1.03$ mm.

	U_{air} (m/s)	T_{air} (K)	$\langle X_{IGN} \rangle$ (mm)	$\sigma_{x,ign}$ (mm)	$\sigma_{y,ign}$ (mm)	$(2D_{tt})^{1/2}$ (mm)
Run 5	15.92	884	31.50	4.05	3.01	2.75
Run 6	19.50	885	38.16	5.07	4.39	3.03
Run 7	20.50	885	38.28	6.31	3.74	3.03
Run 8	22.87	884	45.21	7.34	3.01	3.29
Run 9	29.64	885	45.72	6.39	4.73	3.32

List of Figures

1	Apparatus sketch.	24
2	Typical photographs of acetylene autoignition. (a) $T_{air}=832$ K, $U_{air}=10.9$ m/s, $U_{fuel}=10.9$ m/s, $Y_{fuel}=0.7$, exposure time: 100 ms. (b) $T_{air}=877$ K, $U_{air}=24.5$ m/s, $U_{fuel}=22.1$ m/s, $Y_{fuel}=0.7$, exposure time: 250 ms. (c) Long-exposure photograph of the flow of (a).	25
3	Sequential images of “random spots” of acetylene taken at 6.9 kHz with the small injector ($d=1.03$ mm). Conditions: $T_{air}=885$ K, $U_{air} = U_{fuel}=20.6$ m/s, and $Y_{fuel}=0.78$. The flow is from left to right and the imaged region corresponds to about 70 x 21 mm. The white arrows show examples of internal reflections of the light emitted from the ignited region. Qualitatively identical phenomena were observed for all injectors, fuels, and conditions in the “Random Spots” regime.	26
4	Minimum autoignition lengths for acetylene as a function of (a) U_{air} , (b) T_{air} , for the indicated fuel mass fraction. For all, $U_{fuel}/U_{air} = 1 \pm 0.05$ and $d=2.27$ mm.	27
5	Minimum autoignition lengths for heptane as a function of T_{air} and the indicated U_{air} . For all, $U_{fuel}/U_{air} = 1 \pm 0.05$ and $Y_{fuel}=0.94$ and $d=2.27$ mm.	27
6	(a) Typical OH* profile of an autoignition event with acetylene. Conditions: $T_{air}=807$ K, $T_{fuel}=761$ K, $U_{air} = U_{fuel}=11.1$ m/s, $Y_{fuel}=0.63$, and $d=2.27$ mm. (b) Averaged profiles from various conditions. (c) Selection of images from a typical fast-camera sequence taken at 15 kHz for the conditions of (a).	28
7	Typical simultaneous PMT and microphone signals with acetylene. (a) Chemiluminescence – Slow Spotting Regime ($T_{air}=834$ K, $U_{air}=16.1$ m/s). (b) Chemiluminescence – Fast Spotting Regime ($T_{air}=843$ K, $U_{air}=12.9$ m/s). (c) Pressure – Slow Spotting Regime. (d) Pressure – Fast Spotting Regime. For all, $Y_{fuel}=0.63$ and $d=2.27$ mm.	28
8	(a) Mean and (b) standard deviation divided by the mean of global chemiluminescence intensity as a function of X_{MIN} . $U_{air} = U_{fuel}=11.1$ m/s (circles) and $U_{air} = U_{fuel}=17.5$ m/s (squares), with T_{air} in the range 807-825 K and 851-880 respectively. For all, acetylene with $Y_{fuel}=0.63$ was used.	29

9	(a) Probability density functions of Δt_{ign} and (b) $1/\langle\Delta t_{ign}\rangle$ as a function of X_{MIN} for the conditions of Fig. 8. The inset in (a) shows the same data, but with the x -axis normalized by the corresponding mean $\langle\Delta t_{ign}\rangle$	29
10	(a) Autocorrelation functions of OH* and (b) integral and Taylor timescales for the conditions of Fig. 8.	30
11	Scatter plot of heptane autoignition spots for the indicated T_{air} . $Y_{fuel}=0.94$, $d=2.27$ mm. Left: $U_{air}=18$ m/s. Right: $U_{air}=13.7$ m/s. See Table 1 for the corresponding mean and r.m.s. ignition location results.	30

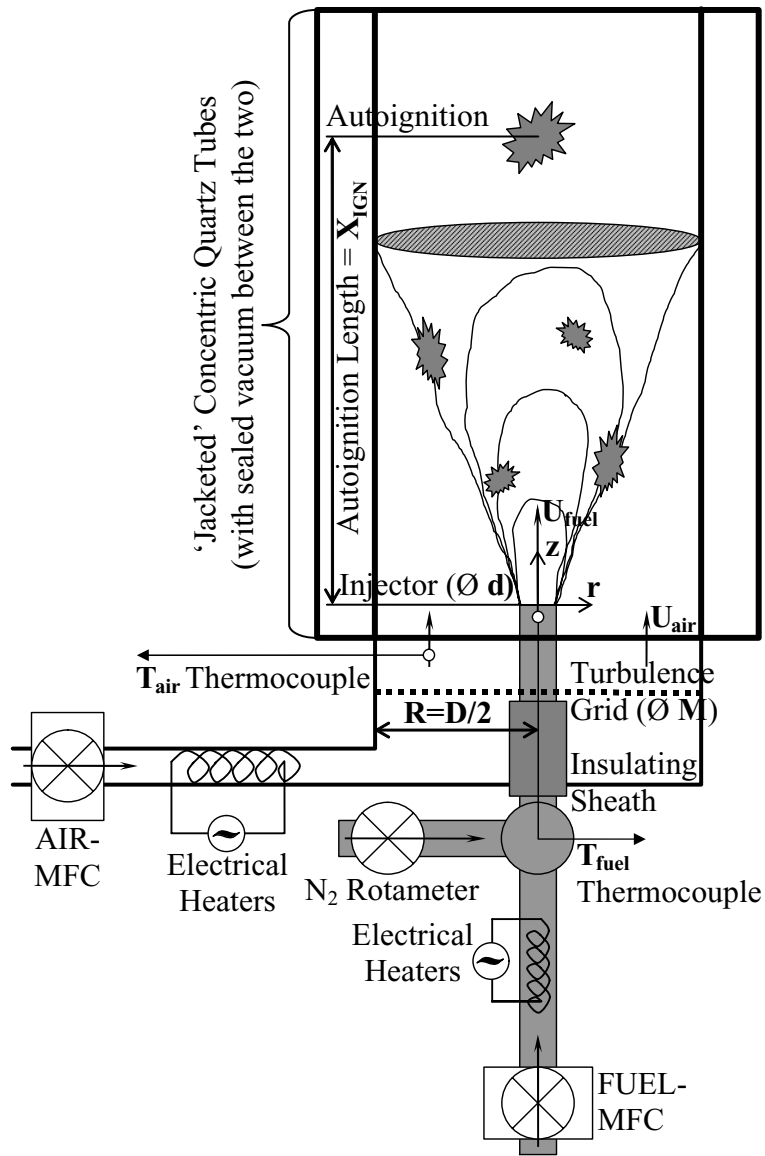


Figure 1: Apparatus sketch.

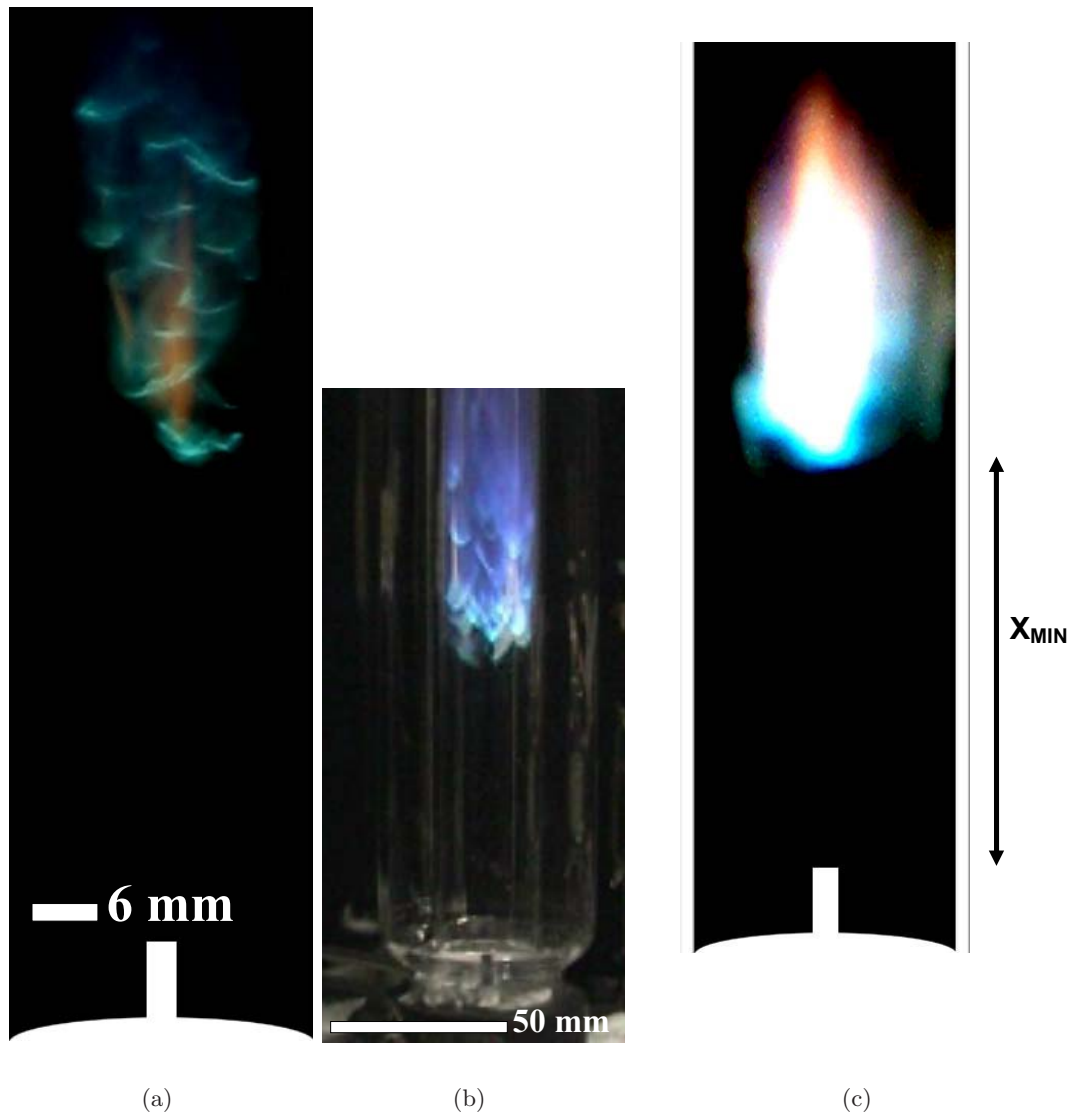


Figure 2: Typical photographs of acetylene autoignition. (a) $T_{air}=832$ K, $U_{air}=10.9$ m/s, $U_{fuel}=10.9$ m/s, $Y_{fuel}=0.7$, exposure time: 100 ms. (b) $T_{air}=877$ K, $U_{air}=24.5$ m/s, $U_{fuel}=22.1$ m/s, $Y_{fuel}=0.7$, exposure time: 250 ms. (c) Long-exposure photograph of the flow of (a).

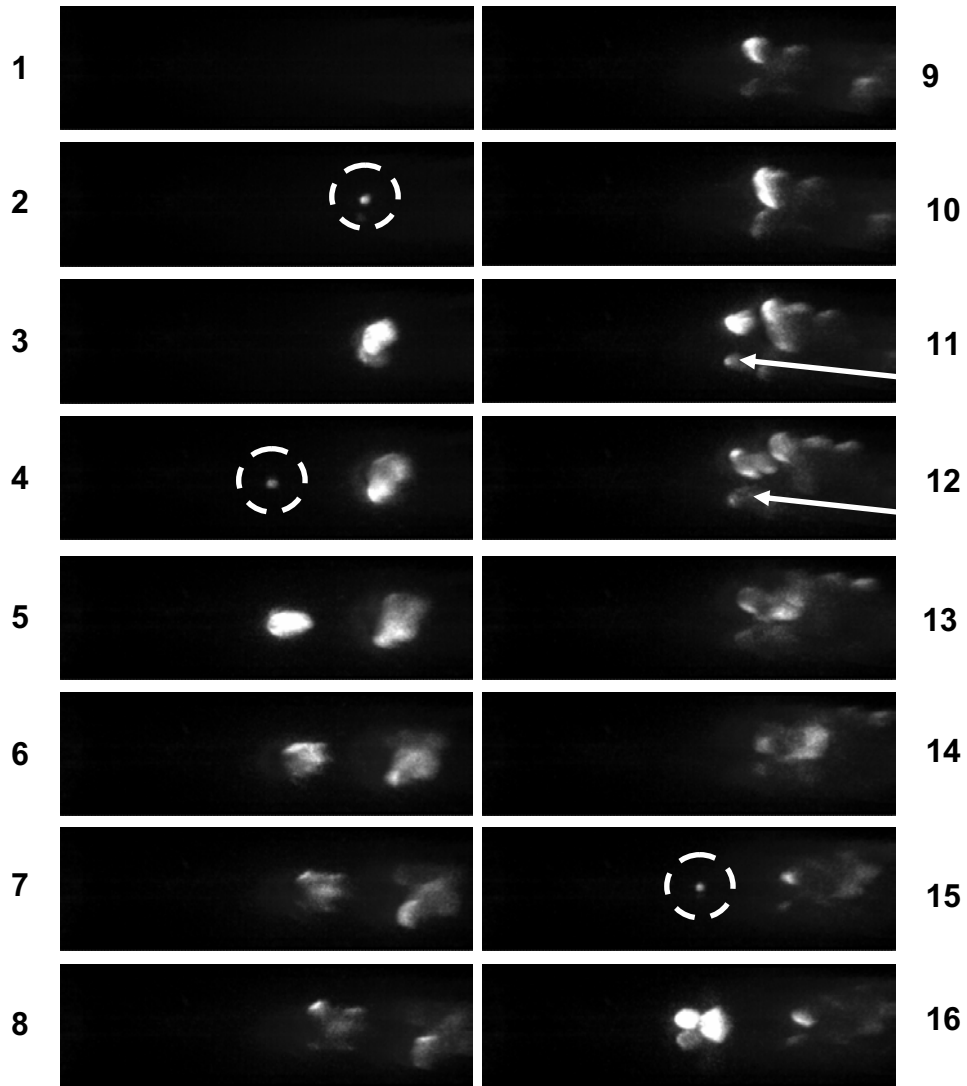


Figure 3: Sequential images of “random spots” of acetylene taken at 6.9 kHz with the small injector ($d=1.03$ mm). Conditions: $T_{air}=885$ K, $U_{air} = U_{fuel}=20.6$ m/s, and $Y_{fuel}=0.78$. The flow is from left to right and the imaged region corresponds to about 70×21 mm. The white arrows show examples of internal reflections of the light emitted from the ignited region. Qualitatively identical phenomena were observed for all injectors, fuels, and conditions in the “Random Spots” regime.

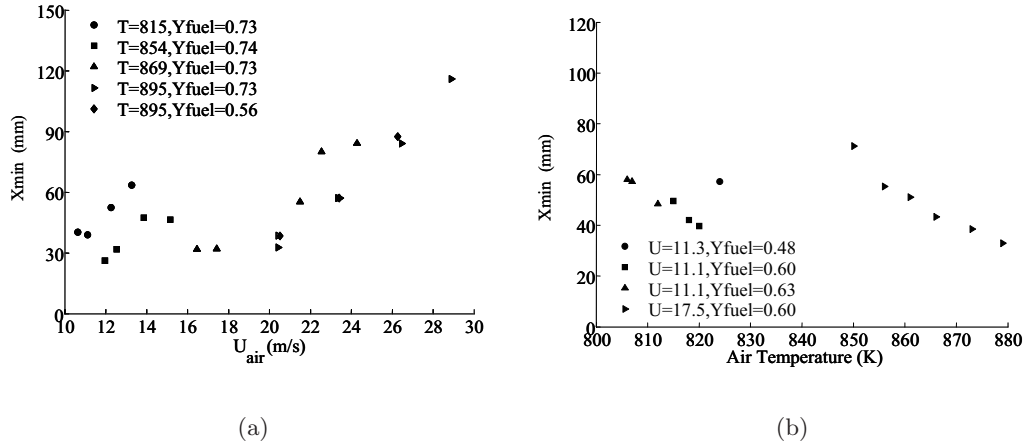


Figure 4: Minimum autoignition lengths for acetylene as a function of (a) U_{air} , (b) T_{air} , for the indicated fuel mass fraction. For all, $U_{fuel}/U_{air} = 1 \pm 0.05$ and $d=2.27$ mm.

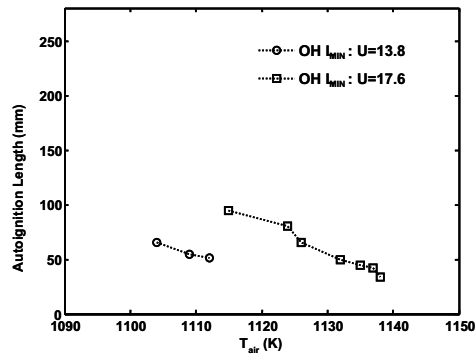


Figure 5: Minimum autoignition lengths for heptane as a function of T_{air} and the indicated U_{air} . For all, $U_{fuel}/U_{air} = 1 \pm 0.05$ and $Y_{fuel}=0.94$ and $d=2.27$ mm.

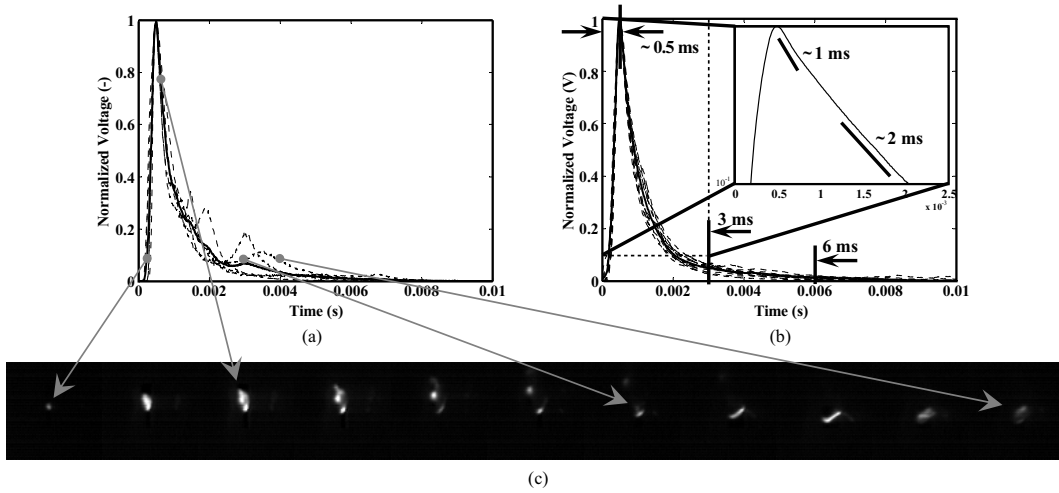


Figure 6: (a) Typical OH* profile of an autoignition event with acetylene. Conditions: $T_{air}=807$ K, $T_{fuel}=761$ K, $U_{air} = U_{fuel}=11.1$ m/s, $Y_{fuel}=0.63$, and $d=2.27$ mm. (b) Averaged profiles from various conditions. (c) Selection of images from a typical fast-camera sequence taken at 15 kHz for the conditions of (a).

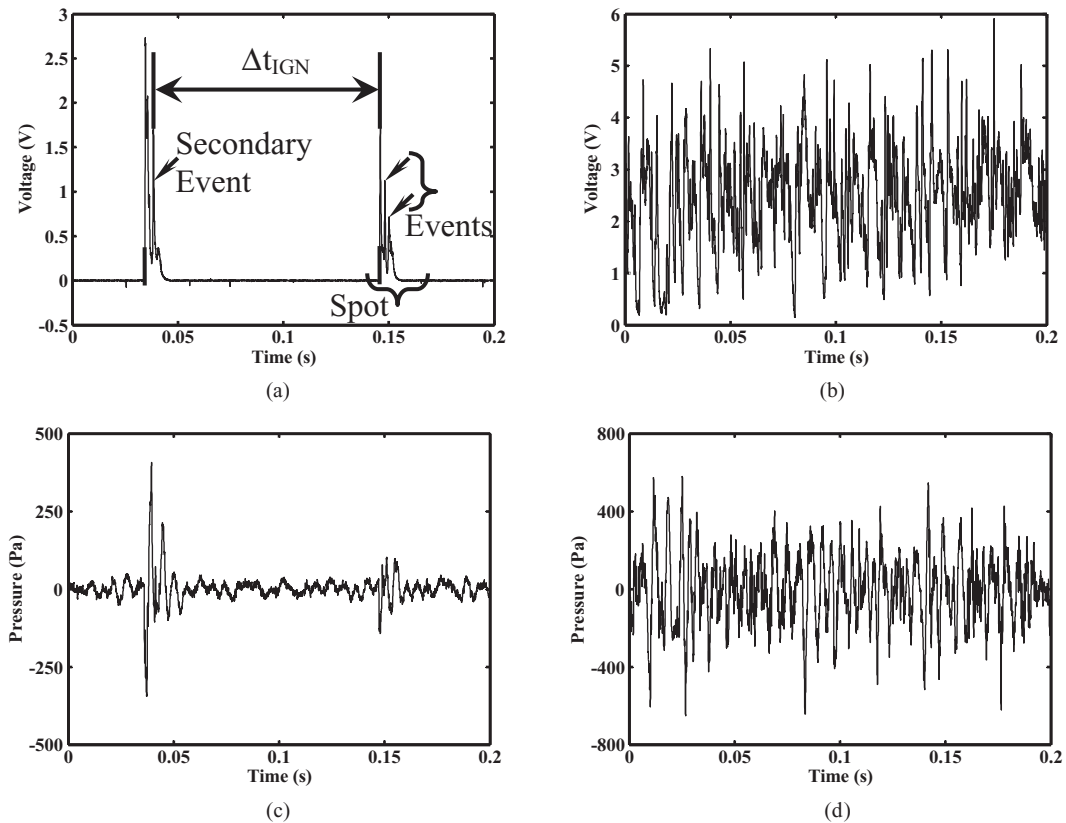


Figure 7: Typical simultaneous PMT and microphone signals with acetylene. (a) Chemiluminescence – Slow Spotting Regime ($T_{air}=834$ K, $U_{air}=16.1$ m/s). (b) Chemiluminescence – Fast Spotting Regime ($T_{air}=843$ K, $U_{air}=12.9$ m/s). (c) Pressure – Slow Spotting Regime. (d) Pressure – Fast Spotting Regime. For all, $Y_{fuel}=0.63$ and $d=2.27$ mm.

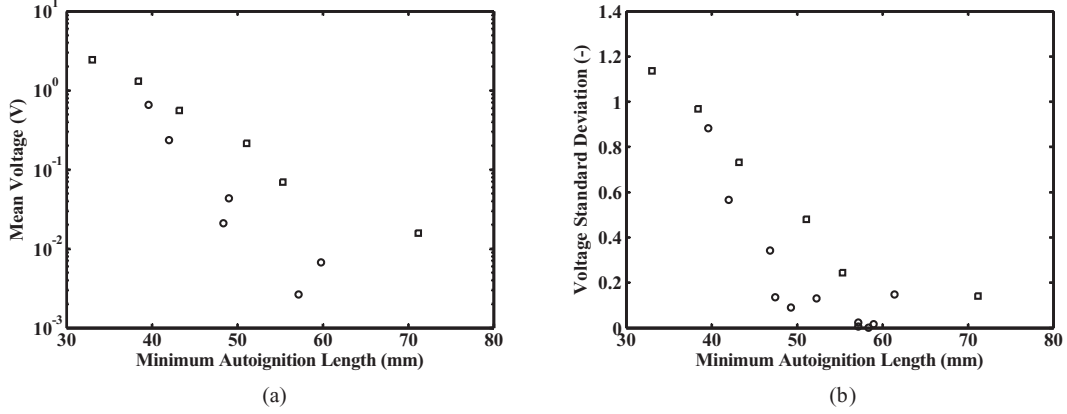


Figure 8: (a) Mean and (b) standard deviation divided by the mean of global chemiluminescence intensity as a function of X_{MIN} . $U_{air} = U_{fuel} = 11.1$ m/s (circles) and $U_{air} = U_{fuel} = 17.5$ m/s (squares), with T_{air} in the range 807-825 K and 851-880 K respectively. For all, acetylene with $Y_{fuel} = 0.63$ was used.

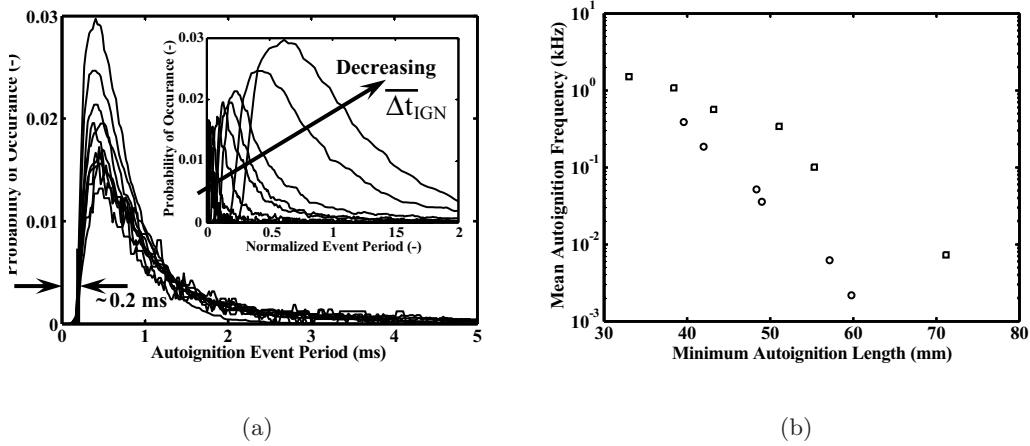


Figure 9: (a) Probability density functions of Δt_{ign} and (b) $1/\langle \Delta t_{ign} \rangle$ as a function of X_{MIN} for the conditions of Fig. 8. The inset in (a) shows the same data, but with the x -axis normalized by the corresponding mean $\langle \Delta t_{ign} \rangle$.

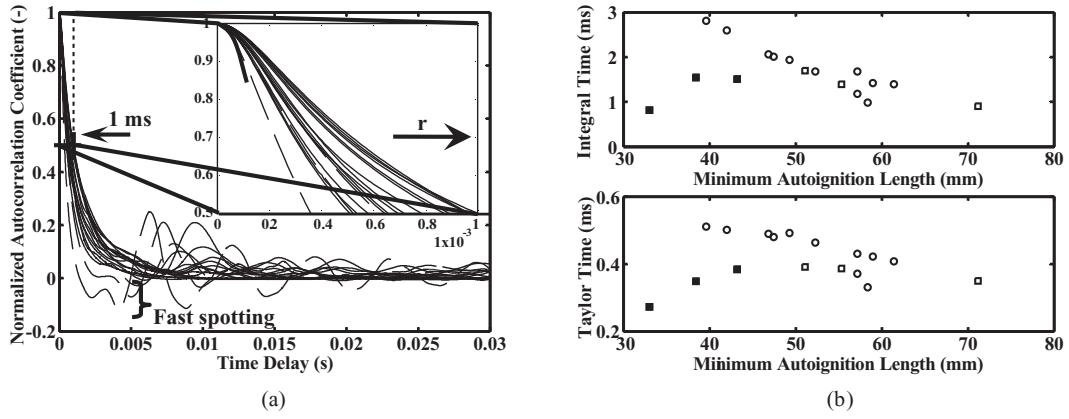


Figure 10: (a) Autocorrelation functions of OH^* and (b) integral and Taylor timescales for the conditions of Fig. 8.

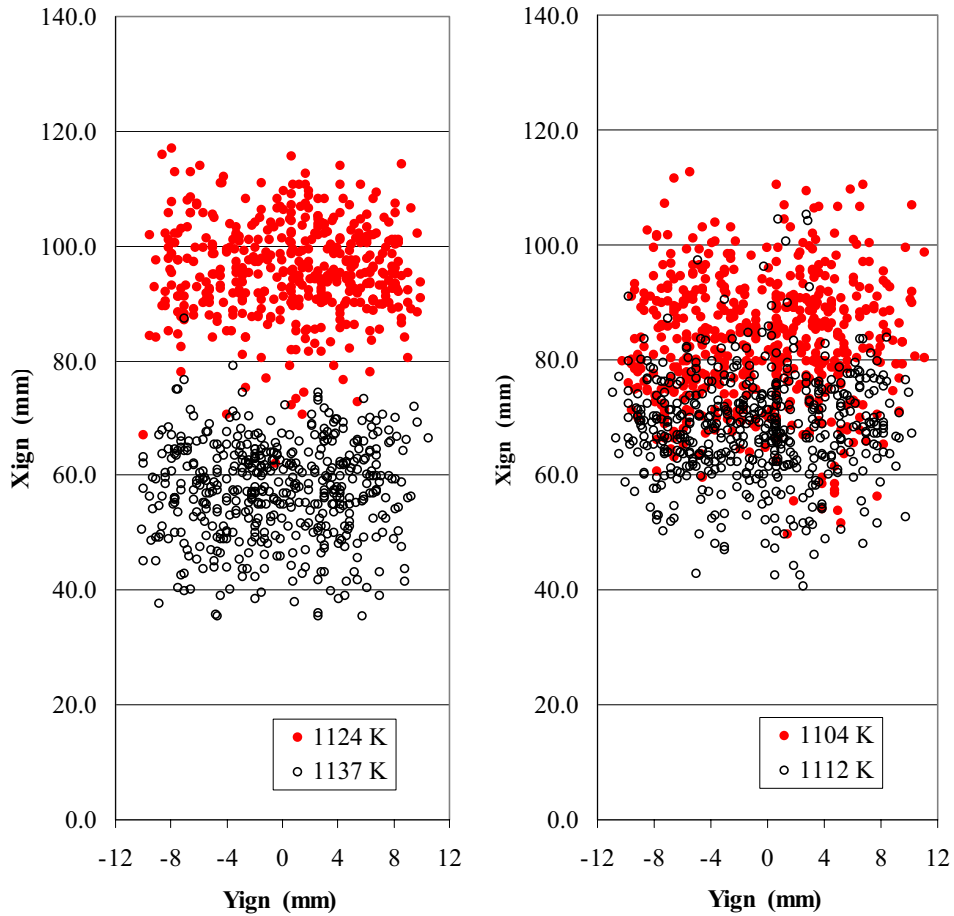


Figure 11: Scatter plot of heptane autoignition spots for the indicated T_{air} . $Y_{fuel}=0.94$, $d=2.27$ mm. Left: $U_{air}=18$ m/s. Right: $U_{air}=13.7$ m/s. See Table 1 for the corresponding mean and r.m.s. ignition location results.